seen. For specimens with increasing Zn content the photon energy of the peak increases (Fig. 3). This is in agreement with results obtained by Biondi and Rayne[18] and theoretical considerations by Lettington[19] and Amar, Johnson, and Sommers.[20] Investigations using higher photon energies and other materials are in progress.

We are indebted to Dr. J. Slater and Dr. J. Conklin for helpful comments.

[1]H. Ehrenreich and H. R. Philipp, Phys. Rev. 128, 1622 (1962).

[2]H. Ehrenreich, H. R. Philipp, and D. J. Olechna, Phys. Rev. 131, 2469 (1963).

[3]H. Ehrenreich, H. R. Philipp, and B. Segall, Phys. Rev. 132, 1918 (1963).

[4]B. R. Cooper, H. Ehrenreich, and H. R. Philipp, Phys. Rev. 138, A494 (1965).

[5]H. Ehrenreich, in *Proceedings of the International Colloquium on Optical Properties and Electronic Structure of Metals and Alloys, Paris, 1965*, edited by F. Abelès (North-Holland, Amsterdam, 1966).

[6]H. Ehrenreich, IEEE Spectrum 2, 162 (1965).

[7]H. R. Philipp and H. Ehrenreich, Phys. Rev. Lett. 8, 92 (1962).

[8]B. Segall, Phys Rev. 125, 109 (1962), and 124, 1797 (1961).

[9]G. A. Burdick, Phys. Rev. 129, 138 (1963).

[10]J. G. Hanus, Massachusetts Institute of Technology Solid State and Molecular Theory Group Quarterly Progress Report No. 44, 1962 (unpublished), p. 29.

[11]See for example M. Cardona, in *Solid State Physics*, edited by H. Ehrenreich, F. Seitz, and D. Turnbull (Academic, New York, 1969), Suppl. 11.

[12]W. E. Engeler, H. Fritzsche, M. Garfinkel, and J. J. Tiemann, Phys. Rev. Lett. 14, 1069 (1965).

[13]U. Gerhardt, Phys. Rev. 172, 651 (1968).

[14]B. O. Seraphin and R. B. Hess, Phys. Rev. Lett. 14, 138 (1965).

[15]C. N. Berglund, J. Appl. Phys. 37, 3019 (1966).

[16]J. Hanus, J. Feinleib, and W. J. Scouler, Phys. Rev. Lett. 19, 16 (1967).

[17]Ref. 11, p. 19.

[18]M. A. Biondi and J. A. Rayne, Phys. Rev. 115, 1522 (1959).

[19]A. H. Lettington, Phil. Mag. 11, 863 (1965).

[20]H. Amar, K. H. Johnson, and C. B. Sommers, Phys. Rev. 153, 655 (1967).

SWITCHING AND TEMPERATURE EFFECTS IN LATERAL FILMS OF AMORPHOUS SILICON*

John E. Fulenwider
General Telephone & Electronics Laboratories, Bayside, New York 11360

and

Gerald J. Herskowitz
Department of Electrical Engineering, Stevens Institute of Technology, Hoboken, New Jersey 07030

(Received 4 May 1970)

Self-heating in films of amorphous silicon prior to switching results from application of voltage pulses producing lateral currents. A smooth, rapid, and highly localized temperature rise always precedes the switching event resulting in a filamentary formation bridging the gap. The negative electrode edge is hotter than the positive electrode edge, and the measured filament temperatures compare favorably with temperatures calculated assuming intrinsic conduction takes place in the confined dimensions of the filament channel.

Electrical switching phenomena reported for thin films of amorphous silicon sandwiched between titanium electrodes[1] bears strong similarity to the behavior exhibited[2,3] by mixtures of chalcogenide glassy semiconductors. For silicon it was reported that memory switching is prevalent with ac excitation; a current-voltage characteristic is produced having a high-resistance region linked through a region of negative differential resistance to a low-resistance region. Two conductivity states, high and low, are reported to exist for chalcogenides; transition from one to the other occurs in short time intervals. Upon switching from the low-conductivity state in both the silicon and chalcogenide glass devices, craters or pits in the electrodes are reported which are attributed to filament path formation. For those chalcogenide materals exhibiting memory switching, the ends of filaments are clearly shown[4] by some observers and by others the filaments are displayed from the side.[5] Recent infrared viewer observations[6] on a chalcogenide glass semiconductor reveal a 650-800°C filament during threshold switching.

Reported here are observations of electrical and thermal measurements made on films of amorphous silicon, electron-beam evaporated on pairs of thermally evaporated nickel electrodes separated by narrow gaps. The configuration is shown in Fig. 1, inset. The silicon exhibits the threshold switching as well as the memory switching effects reported above. An infrared microradiometer (Barnes Engineering Company model RM2A) was used to observe radiance emitted from the silicon surface in response to dc testing pulses applied through a mercury-wetted relay (C. P. Clare model HG2A) from a regulated power supply. Signals from the microradiometer were amplified and displayed on an oscilloscope (Tektronix model 547 with 1A4 amplifier). Corrections for silicon emissivity (measured value 0.47) and aperture effect have been made. Resolution of the infrared reflection optics at 15× objective is 0.0014 in., and the aperture function was determined to be approximately Gaussian.

Electron diffraction studies of the silicon film verified its amorphous nature; there is no evidence of crystallites greater than 10 Å. Platinum-shadowed surface replicas of the silicon also disclose lack of structure; at 134 000× it is reminiscent of an expanse of finely shredded tobacco.

Initial room-temperature resistance of the silicon lies in the range of 400 to 700 Ω cm as determined by four-point probe measurements, and also by an ohmmeter connected across the nickel electrodes. Electrode gaps and silicon widths and thicknesses (in the range of 0.8 to 1.3 μm) established initial dc room-temperature resistances; Ohmic contacts prevail. Measurements of the logarithm of resistivity versus $1/T$ were found to be in agreement with the results of Grigorovici.[7] Capacitance of the test configurations lies in the range of 0.28 to 0.38 pF. Seebeck voltages at room temperature measure between 15 to 30 μV/°K, p type, also in agreement with data obtained by Grigorovici.

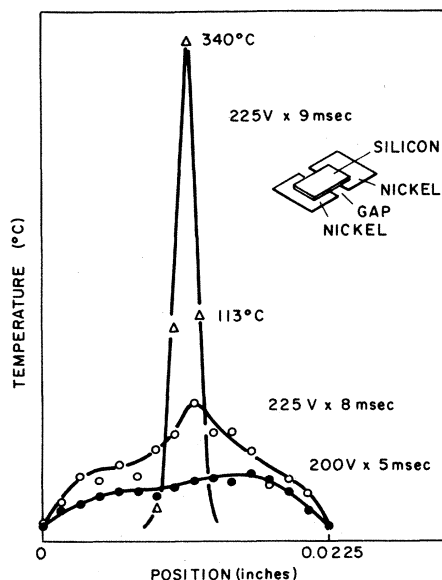

FIG. 1. Effective blackbody temperature versus position along midline of gap. Width of sample is 0.0225 in., gap is 25 μm, film thickness 0.8 μm (vertical scale is nonlinear). Inset depicts typical configuration of samples tested.

In response to an applied rectangular voltage pulse the temperature in the silicon rises rapidly from room temperature (25°C) to some peak value depending on applied voltage, device initial resistance, and duration of the pulse, and then falls to room temperature shortly (typically less than 5 msec) after cessation of the pulse. A sufficiently large rectangular pulse causes the silicon to sustain a switching event, not taking place instantaneously with application of the pulse but delayed for a time interval (incubation time). Temperature is observed to rise during this interval, and its rate of rise increases such that at the transition time it has reached an estimated 1400°C; a filamentary channel forms, widens, and cools – all within nanoseconds – to a measured temperature in the range of 300 to 400°C where silicon intrinsic conductivity for the measured filament dimensions substantiates the measured device resistance. Table I compares typical measured filament temperatures with those calculated from filament dimensions using $\log\rho$ vs $1/T$ for the material. It shows general agreement between measured temperature and that deduced from intrinsic conductivity. Ratios of the dc resistance before switching to the resistance (V/I) after switching lie in the range 40:1 to 8:1.

The filamentary channel which forms appears to bridge the gap between the electrode edges. All filaments observed have tapered ends where they join the electrodes. They are approximately 0.8 μm wide at the ends, and 5 μm wide at the midpoints. While conducting after the switching event the temperature of the negative-electrode end of the filament is approximately 1200°C; the positive-electrode end is approximately 980°C; and the body of the filament approximately 350°C. X-ray analysis of switched samples containing filaments reveals traces of nickel-silicon com-

Table I. Data on filament resistivity and temperature characteristics.

Filament length[a] (μm)	Resistance (Ω)	Resistivity (Ω cm)	Temperature corresponding to intrinsic resistivity (°C)	Measured temperature (°C)
25	13 360	0.2135	335	340
25	43 300	0.6920	302	271[b]
25	13 360	0.213	362	377
50	9200	0.0736	315	302
50	19 500	0.312	332	323[b]
50	24 900	0.199	340	270[b]
15	15 300	0.408	324	350
15	15 300	0.408	322	393
50	13 900	0.111	361	355
50	8350	0.0667	384	370

[a]Width 5.0 μm, thickness 0.8 μm.

[b]Threshold switching; the remainder are memory type.

pounds; those that have not switched reveal no nickel. The analysis is so far inconclusive regarding crystallization of the silicon in the filament. Typical current densities at the filament–negative-electrode interface lie in the range of $(4.0 \text{ to } 5.0)\times 10^5$ A/cm^2.

Every filament that forms in response to a large test pulse forms at the location which exhibits the largest transient rise in temperature in response to the smaller testing pulses previously applied. A smooth and rapid rise in temperature of silicon in the gap becoming locally prominent always precedes the switching event. The localized position of highest temperature coincides with the formation of the filamentary channel. Evidence for a progressively narrowing, rising-temperature channel is derived from the infrared radiaometer scans of switching events in which the bore sight of the microscope viewed a filament forming on center; then in another sample viewed a filament forming off center, and so forth. By observing the radiance from the silicon at regularly spaced sampling positions along the gap midline in response to subswitching test pulses, a temperature contour is obtained. Approximately 16 pulses are required to obtain one contour. Figure 1 shows the result of this plot of the temperature peaks for three sizes of pulses versus position for a typical sample. For the smallest pulse, the temperature contour exhibits a gradient of less than 1300°C/cm, and has a maximum temperature of 53°C near the center. The contour for the intermediate pulse shows a maximum gradient of 2500°C/cm; its maximum is 72°C. For the largest pulse the contour shows that the maximum temperature gradient is about 90 000°C/cm, and the maximum temperature is 340°C. The material represented by this contour switched from low resistance to high resistance in response to the largest test pulse. Scans of the positive and negative edges of the gap in the silicon prior to switching show the negative edge to be of higher temperature than the positive edge. A typical pair of temperatures is 105 to 98°C.

Transition times decrease with a decrease in gap dimension as illustrated in Fig. 2(a). Samples with gaps of 15, 25, and 50 μm were switched; the switching time was determined from the voltage drop across the device. Transition times increase only slightly with an increase in load resistance. Incubation times shown in Fig. 2(b) decrease with increasing input power, measured as the product of the initial peak voltage across the device times the coincident input current.

If the test pulse that is applied to the silicon causes it to switch, the filamentary path which forms will be one of two possible types. A memory filament will form or a threshold filament will form. We observe that a memory filament, while carrying current, at midgap has a temperature greater than that of a threshold filament. This trend is seen in the table. Circuit load resistance and applied voltage magnitude and duration determine these temperatures for fixed device geometry.

Samples were examined in a scanning electron microscope (JELCO model JSM1) at 2000×, while being subjected to a cumulative succession of in-

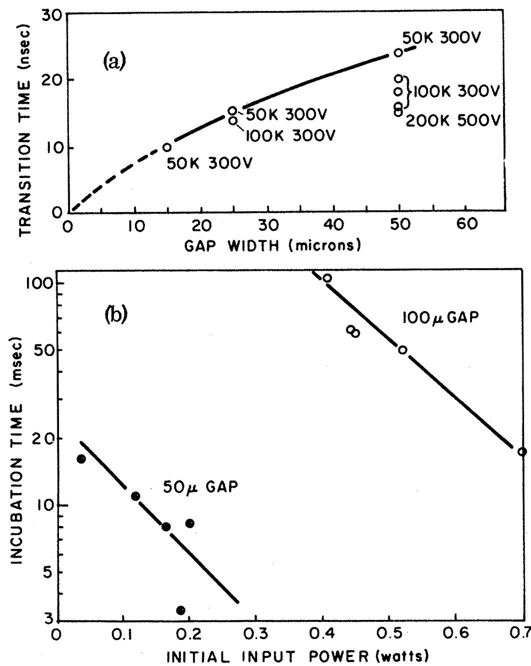

FIG. 2. (a) Transition time (nsec) versus gap width (μm) for 50, 100, and 200 kΩ series load resistors. (b) Incubation time (msec) versus initial input power for 50 and 100 μm gap width samples.

cremental steps of 10 V up to a voltage at which switching occurred. At the time that switching occurs, the resistance of the silicon drops and a channel forms in it. The channel spans between the nickel electrodes, and globular formations lining the sides of the channel are observed, which are suggestive of melting. Channels have tapered ends, and widths at midgap approximately 3 μm.

A comparison is made of current densities, based on estimates of the nickel-silicon filament boundary cross-sectional dimension, with those calculated using a Schottky-barrier thermionic emission equation.[8,9] Assuming reverse-bias, p-type silicon, a temperature of 1473°K at the filament–negative-electrode boundary, $q\varphi_{Bn}$ of 0.64 eV, and $A^{**}=30$ A/(cm °K)^2, one calculates a current density of 4.2×10^5 A/cm^2. The measured current density corresponding to the above negative-electrode temperature is 4.58×10^5 A/cm^2. Considering the difficulty in obtaining an accurate temperature, and an accurate measurement of the nickel-silicon interface area, the agreement is remarkable.

We conclude that the switching phenomenon in these amorphous silicon films is the result of Joule heating produced by the input excitation interacting with the bulk negative temperature coefficient of resistivity of the material. Temperature events leading to current filament formation confirm what Ridley[9] had pointed out for materials having bulk negative temperature coefficient of resistivity, i.e., filamentary current paths will form as the limiting case for these types of materials.

The switching event is the culmination of temperature rising high enough to reach the melting point of the silicon at least momentarily so that metallic conduction takes place; all the device current flows in the filament at that time. As a result of the high temperature some of the nickel at the electrode interface partly dissolves into the silicon. The silicon bordering on the conducting filament receives heat energy from the filament by thermal conduction, driven by the large temperature gradient. The neighboring silicon can become part of the conducting path, and it will widen until the necessary heat balance between generation and loss is satisfied. Radiation plays a minor role. The higher thermal conductivity of nickel compared with that of silicon may explain the narrower cross section observed at the nickel-filament interface compared with the filament body, since the nickel at these dimensions is about 3 times as thermally conductive as the silicon.

The authors wish to thank F. LiDonni, F. Marchese, and E. Bulan for their help in fabrication of the devices, Mr. C. Tufts, M. Downey, and J. Varon for electron microscope, x-ray, and scanning electron microscope examinations, and E. M. Conwell for helpful discussions during this work.

---

*Research supported by GT&E Labs, Inc., research fellowship.

[1]D. Feldman, and K. Moorjani, in *Proceedings of the Symposium on Semiconductor Effects in Amorphous Solids*, edited by W. Doremus (North-Holland, Amsterdam, 1970), p. 82.

[2]S. R. Ovshinsky, Phys. Rev. Lett. 21, 1450 (1968).

[3]R. R. Shanks, in *Proceedings of the Symposium on Semiconductor Effects in Amorphous Solids*, edited by W. Doremus (North-Holland, Amsterdam, 1970), p. 504.

[4]A. D. Pearson, and C. E. Miller, Appl. Phys. Lett. 14, 9 (1969).

[5]N. J. Stocker, in *Proceedings of the Symposium on Semiconductor Effects in Amorphous Solids*, edited by W. Doremus (North-Holland, Amsterdam, 1970), p. 371.

[6]D. F. Weirauch, Appl. Phys. Lett. 16, 72 (1970).

[7]R. Grigorovici, N. Croitoru, and A. Devenyi, Phys. Stat. Solidi 23, 621 (1967).

[8]C. R. Crowell and S. M. Sze, Solid State Electron. 9, 1035 (1966).

[9]S. M. Sze, *Physics of Semiconductor Devices* (Wiley, New York, 1969), p. 400.

SUSCEPTIBILITY OF PARAMAGNETIC Ni-Cu ALLOYS

Moshe Fibich and Amiram Ron
Dapartment of Physics, Technion-Israel Institute of Technology, Haifa, Israel
(Received 15 April 1970)

A model for paramagnetic Ni-Cu alloys is proposed, wherein magnetic clusters with giant moment ($\sim 10\mu_B$) interact via the itinerant electrons. The interaction is shown to oscillate in space with a wavelength of the order of the cluster size. A Curie-Weiss susceptibility results in θ becoming negative (antiferromagnetic interaction) at low Ni concentration.

Ni_xCu_{1-x} alloys have been studied extensively over a wide range of x, the atomic Ni concentration. On the ferromagnetic side of the critical composition ($x > 0.44$) neutron-scattering,[1] high-temperature susceptibility,[2] and saturation-moment[3,4] measurements indicate that a magnetic clustering phenomenon occurs. The clusters are spin-polarization clouds which are formed in local Ni-rich regions of the random alloy.

Recently Kouvel and Comly[5] extended these measurements into the paramagnetic region of Ni concentration ($0.32 < x < 0.44$). From their bulk magnetization measurements they find that the zero-field susceptibility χ_0 has the form

$$\chi_0 = \chi' + B/(T-\theta). \tag{1}$$

In Eq. (1), χ' is essentially independent of temperature and Ni concentration. In the Curie-Weiss term, B and θ decrease with decreasing Ni concentration, and in particular θ becomes negative (indicating antiferromagnetic interaction between clusters) below $x \sim 0.39$. Attributing the Curie-Weiss susceptibility to the interacting clusters, it follows that $B = CM/3k$, where M is the magnetic moment per cluster and C is the cluster concentration (number of clusters per atom). Using saturation-moment data extrapolated to zero field (which gives NCM), they conclude that M is fairly constant, $(10\text{-}12)\mu_B$, consistent with the moment deduced from neutron scattering in the weakly ferromagnetic alloys.[1]

To account for the Curie-Weiss susceptibility and for the variation of θ with x, we propose a model of localized magnetic clusters interacting via the itinerant electrons. The clusters are randomly distributed in the alloy, each one extending over a large number of neighboring sites (12-20). The itinerant electrons interact with the magnetic moment of each cluster as a whole, rather than with its atomic constituents. Thus, the interaction Hamiltonian is

$$H_{\text{int}} = \sum_n \sum_i J(\vec{R}_n - \vec{r}_i)\vec{S}_n \cdot \vec{s}(\vec{r}_i). \tag{2}$$

Here $\vec{R}_n$ are the (random) coordinates of the (center of the) nth cluster, and $\vec{r}_i$ the coordinates of the itinerant electrons. $\vec{S}_n$ is the nth cluster spin operator and $\vec{s}(\vec{r}_i)$ the spin operator of the itinerant electrons. $J(\vec{R}_n - \vec{r}_i)$ is the interaction coupling and has a finite range in space, of the order of the cluster size. In terms of the electron spin-density operator

$$\vec{s}(\vec{q}) = \int \frac{d^3p}{(2\pi)^3} \sum_{\alpha\beta} \vec{\sigma}_{\alpha\beta} c_{\vec{p}+\vec{q},\alpha}{}^\dagger c_{\vec{p},\alpha}, \tag{3}$$

we rewrite Eq. (2) as

$$H_{\text{int}} = \int \frac{d^3q}{(2\pi)^3} J(\vec{q}) \sum_n \vec{S}_n \cdot \vec{s}(\vec{q}) e^{i\vec{q}\cdot\vec{R}_n}. \tag{4}$$

In Eq. (3), $\vec{\sigma}_{\alpha\beta}$ are the Pauli spin matrices, and $c^\dagger$ and c the itinerant electron creation and annihilation operators.

The cluster spin susceptibility can be expressed by

$$\chi = \sum_{n,m} \chi_{nm}, \tag{5}$$

where the sum extends over the cluster coordinates. χ_{nm} is the time integral of the correlation $\langle [S_n(t), S_m(0)] \rangle$ and is shown diagramatically in Fig. 1. The shaded bubble represents χ_{nm}, the open bubble represents $\chi_{nm}{}^0$ (the paramagnetic spin susceptibility of noninteracting spins), and the wiggly line represents $V_{n'm'}$, the effective cluster-cluster interaction (located at $\vec{R}_{n'}$ and $\vec{R}_{m'}$, respectively). The diagram in Fig. 1 corresponds to the integral equation

$$\chi_{nm} = \chi_{nm}{}^0 + \sum_{n'm'} \chi_{nn'}{}^0 V_{n'm'} \chi_{m'm}, \tag{6}$$